STRUCTURAL CONTROL AND HEALTH MONITORING
Struct. Control Health Monit. 2007; **14**:144–161
Published online 12 October 2005 in Wiley InterScience (www.interscience.wiley.com). DOI: 10.1002/stc.116

Unsupervised fuzzy neural networks for damage detection of structures

C. M. Wen, S. L. Hung*,†, C. S. Huang and J. C. Jan

Department of Civil Engineering, National Chiao Tung University, 1001 Ta Hsueh Road, Hsinchu, Taiwan 300, R.O.C.

SUMMARY

This work presents an artificial neural network (ANN) approach for detecting structural damage. In place of the commonly used supervised neural network, this work adopts an unsupervised neural network which incorporates the fuzzy concept (named the unsupervised fuzzy neural network, UFN) to detect localized damage. The structural damage is assumed to take the form of reduced elemental stiffness. The damage site is demonstrated to correlate with the changes in the modal parameters of the structure. Therefore, a feature representing the damage location, termed the damage localization feature (DLF) is presented. When the structure experiences damage or change in the structural member, the measured DLF is obtained by analyzing the recorded dynamic responses of the structure. The location of the structural damage then can be identified using the UFN according to the measured DLF information. This study verifies the proposed model using an example involving a five-storey frame building. Both single- and multiple-damaged sites are considered. The effects of measured noise and the use of incomplete modal data are introduced to inspect the capability of the proposed detection approach. Additionally, the simulation results of well-known back-propagation network (BPN) and UFN are compared. The analysis results indicated that the use of fuzzy relationship in UFN made the detection of structural damage more robust and flexible than the BPN.

KEY WORDS: unsupervised fuzzy neural network; damage detection; BPN

1. INTRODUCTION

Owing to improved instrumentation and understanding of the dynamics of the complex structures, efforts to identify structural damage have received increasing attention recently. Although potential applications have been achieved [1–3], damage assessment for complex civil engineering structures remains problematic [4]. Among many damage detection techniques, the vibration-based approach is promising because it is nondestructive and the vibration signal of a

*Correspondence to: Professor Shih-Lin Hung, Department of Civil Engineering, National Chiao Tung University, 1001 Ta Hsueh Road, Hsinchu, Taiwan 300, R.O.C.
†E-mail: slhung@mail.nctu.edu.tw

Contract/grant sponsor: National Science Council, R.O.C.; contract/grant number: NSC90-2211-E-009-031

Received 22 December 2004
Revised 22 July 2005
Accepted 4 August 2005

structure is easily measurable using properly deployed sensors. During the last two decades, various vibration-based methods have been developed and applied to detect structural damage in numerous areas. These methods are based on the fact that structural damages reduce the structural stiffness, changing the dynamic structure characteristics (such as modal parameters) of the structures. Analysis of the dynamic responses to obtain the modal parameters of the structure before and after the occurrence of damage can diagnose the existence and extent of structural damage.

Structural damage detection methods used natural frequencies to indicate damage in earlier research. Cawley and Adams [5] proposed the first model by employing the changes in natural frequencies, combined with a finite element model (FEM), to locate sites of damage on a given structure. Following their results, some investigations [6–9] found this method susceptible to measurement errors, and methods of improving the damage localization have been introduced. However, the frequencies are not spatially specific, nor are they sensitive to damage, thus limiting their application. Since mode shapes can provide much more information than natural frequencies, many studies have focused on damage detection using mode shape information [10–12]. Topole and Stubbs [13] used natural frequencies with mode shapes and demonstrated the importance of introducing mode shape orthogonality to identify the location and extent of structural damage. Recently, Shi *et al*. [14] developed a sensitivity and statistically based method for localizing structural damage by using incomplete mode shapes. The damage detection strategy involves first localizing the damage sites by using incomplete measured mode shapes, and then detecting the site and extent of damage using the more accurate measured natural frequency information.

Another set of techniques for detecting structural damage use change in modal strain energy. Hearn and Testa [15] illustrated that the ratio of elemental strain energy to total kinetic energy for the system is a fraction of the eigenvalue, and the ratio of this fraction for two different modes depends only on the damage location. Shi *et al*. [16] developed a method based on modal strain energy for locating structural damage. This method uses the change in modal strain energy in each structural element before and after the occurrence of damage. Some properties of the modal strain energy change are provided to illustrate its sensitivity of locating damage.

Owing to the features of robustness, fault tolerance, and powerful computational ability, the ANN models have become a promising tool for solving civil engineering problems. Masri *et al*. [17] demonstrated that neural networks are a powerful tool for identifying systems typically encountered in structural dynamics. Some researches have examined the suitability and capabilities of ANNs for damage detection. Ghaboussi *et al*. [18] and Wu *et al*. [19] trained neural networks to recognize the frequency response characteristics of undamaged and damaged structures. The various damage levels were simulated by adjusting the properties of individual members. Elkordy [20] used an FEM to design failure patterns that were used to train a neural network to subsequently diagnose damage in the reference structure. Zhao *et al*. [21] designed a neural network approach based on mapping the static equilibrium requirement for a structure in a finite element formulation based on the assumption that structural damage is reflected in terms of stiffness reduction. The analytic results revealed that, even with input noise and incomplete measured data, ANNs can still obtain a satisfactory diagnosis. Masri *et al*. [22, 23] used ANN-based approaches to detect changes in the characteristics of systems whose structures were unknown. Their approaches rely on using vibration measurements from 'healthy' systems to train a neural network for identification purposes. Subsequently, the trained network is fed comparable vibration measurements from the same structure under different episodes of

response to monitor structure health. All of these investigations indicated that ANNs provide a powerful tool for assessing the condition of damaged structures.

Consequently, with strong theoretical support and successful applications of ANNs, the damage detection approach proposed in this work is developed using the modal parameters of the structure, and an ANN model with an unsupervised fuzzy reasoning algorithm. This work first introduces a feature representing the damage location, termed damage localization feature (DLF). The background and operation of the UFN then is briefly reviewed. The reasons for the utilization of the unsupervised neural network then are explained in a subsequent section. The damage location can be recognized using the DLF and the UFN reasoning process. This study presents a numerical example of a five-storey frame building damaged at either single or multiple sites, to verify the effectiveness of the proposed approach. Additionally, the influences of measured noise and the use of incomplete modal data are also examined. Meanwhile, the well-known BPN and UFN were compared. The results presented herein indicated that both BPN and UFN are capable of damage localization purpose. However, the use of fuzzy relationship in UFN increased detection robustness and flexibility.

2. IDENTIFICATION OF DAMAGE LOCALIZATION BASED ON THE CHANGES IN MODAL PARAMETERS

Based on recent developments in measuring and data analyzing techniques, natural frequencies and mode shapes of a structural system can easily be obtained through utilizing system identification procedure. Therefore, the damage detection approach has been developed on the basis of the available natural frequencies and mode shapes of the structures.

For an undamaged structure, the modal characteristics can be described by the following eigenvalue equation:

$$[\mathbf{K} - \lambda_i \mathbf{M}]\phi_i = 0 \quad \text{for } i = 1, \ldots, n \tag{1}$$

where λ_i is the ith modal eigenvalue which presents the square of the natural frequency of the structure; ϕ_i is the ith eigenvector which presents the mode shape of the structure; $\mathbf{K}$ and $\mathbf{M}$ are symmetric stiffness and mass matrixes, respectively.

Generally, the damage of a structure is assumed to be the reduction of stiffness in structural elements, then the eigenvalue equation for such a damaged structure becomes

$$[(\mathbf{K} - \Delta\mathbf{K}) - (\lambda_i - \Delta\lambda_i)\mathbf{M}](\phi_i - \Delta\phi_i) = 0 \tag{2}$$

Assume the system stiffness matrix is the combination of individual member stiffness matrices. Thus, the change in stiffness matrix due to damage can be expressed as

$$\Delta\mathbf{K} = \sum_{e=1}^{N_d} \alpha_e \mathbf{k}_e \tag{3}$$

where $\mathbf{k}_e$ is the individual stiffness matrix for the eth element; α_e, which is within the range 0–1, is the coefficient defining a fractional change of the eth elemental stiffness matrix; and N_d is the total number of damaged elements in the structure.

Expanding Equation (2) and neglecting the higher-order terms of Δ yields

$$-\Delta\mathbf{K}\phi_i + \Delta\lambda_i\mathbf{M}\phi_i - \mathbf{K}\Delta\phi_i + \lambda_i\mathbf{M}\Delta\phi_i = 0 \tag{4}$$

Premultiplying Equation (4) with ϕ_i^{T}, the expression for change in eigenvalue is obtained as

$$\Delta\lambda_i = \frac{\phi_i^{\mathrm{T}} \Delta\mathbf{K} \phi_i}{\phi_i^{\mathrm{T}} \mathbf{M} \phi_i} \tag{5}$$

This equation expresses the relationship between the structural damage and the eigenvalue change.

Subsequently, the relationship between the structural damage and the eigenvector change is derived. Pre-multiplying Equation (4) with ϕ_j^{T} leads to the following equation:

$$(\lambda_j - \lambda_i)\phi_j^{\mathrm{T}} \mathbf{M} \Delta\phi_i = -\phi_j^{\mathrm{T}} \Delta\mathbf{K} \phi_i \tag{6}$$

where $\Delta\phi_i$ is assumed to be a linear combination of the mode shapes, i.e.

$$\Delta\phi_i = \sum_{k=1}^{N} c_{ik} \phi_k \tag{7}$$

Substituting Equation (7) into Equation (6), and introducing the orthogonal property, Equation (6) is rearranged as

$$c_{ij} = \frac{-\phi_j^{\mathrm{T}} \Delta\mathbf{K} \phi_i}{(\lambda_j - \lambda_i)\phi_j^{\mathrm{T}} \mathbf{M} \phi_j} \tag{8}$$

Substituting Equation (8) into Equation (6), the expression shows the change in ith eigenvector of the system.

$$\Delta\phi_i = \sum_{j=1}^{N} \frac{-\phi_j^{\mathrm{T}} \Delta\mathbf{K} \phi_i}{(\lambda_j - \lambda_i)\phi_j^{\mathrm{T}} \mathbf{M} \phi_j} \phi_j \tag{9}$$

Equations (5) and (9) clearly show the expression of changes in modal values and vectors, respectively. The changes in modal values and vectors are direct proportion to the stiffness change.

Finally, imposing Equation (3) on Equations (5) and (9), and supposing that single damage or multiple damages with similar severity (i.e. all α_e, $e = 1 \sim N_{\mathrm{d}}$, are identical) exist in the structure, the expression for the change in the ith modal vector divided by the change in the jth modal value (i.e. dividing Equation (9) by Equation (5)) can be obtained as follows:

$$\frac{\Delta\phi_i}{\Delta\lambda_j} = \frac{\sum_{j=1}^{N} \dfrac{-\phi_j^{\mathrm{T}} \sum_{e=1}^{N_{\mathrm{d}}} \mathbf{k}_e \phi_i}{(\lambda_j - \lambda_i)\phi_j^{\mathrm{T}} \mathbf{M} \phi_j} \phi_j}{\dfrac{\phi_j^{\mathrm{T}} \sum_{e=1}^{N_{\mathrm{d}}} \mathbf{k}_e \phi_j}{\phi_j^{\mathrm{T}} \mathbf{M} \phi_j}} \tag{10}$$

Explicitly, Equation (10) depends on damage location only and the term on the left-hand side, termed the damage localization feature (DLF) in this paper, can be used as an indicator for identifying the location of structural damage.

Based on the analytic model (FEM for example) of a real-world structure, the analytic damage localization feature (ADLF) $\Delta\phi_i/\Delta\lambda_j$ for different damage cases can be calculated in advance to construct an ADLF database. With proper deployment of sensors, the vibration signal of the structure can be measured through ambient, free, or forced vibration tests and then the modal parameters can also be generated through the system identification technique [24].

When the measured modal parameters are available, the damage location can then be assessed by matching the measured damage localization feature (MDLF) with the ADLF for different possible damage cases. The damage case with the largest 'similarity' (i.e. the smallest discrepancy) between MDLF and ADLF is identified to be the possible damage on the structure.

3. UNSUPERVISED FUZZY NEURAL NETWORKS (UFN) FOR THE DAMAGE DETECTION OF STRUCTURES

In the studies of damage detection that based on certain damage indices or features, there are two main approaches usually adopted to deal with the detection or diagnosis process. One computed the discrepancy between the measured (or real) damage index and the FEM-based analytic damage index for all potential damage states to a structure. The case with the smallest discrepancy represents the current state for the structure [15, 25]. The other optimizes the specified objective function(s) in which the measured information is included to search for the possible damage state [9]. Accordingly, no matter what approach is adopted, the key point of damage detection is how to rapidly and correctly identify the possible damage state according to the measured data. Therefore, one can establish the damage features for every possible damage states via the analytic FEM. When the measured damage feature is available through measurement, the damage state can then be identified by finding the same or most similar damage features. According to Equation (10) in previous section, the location of damage to a structure is dependant only on the ratio of changes in modal vectors and modal values, and can be identified by matching the MDLF and the ADLF. The process of using DLF to find the damage location is more like pattern classification (or recognition) than functional mapping. Consequently, instead of the most utilized supervised neural network (which is powerful for the functional mapping problems) in the related studies about damage detection or health motoring, this study employs an unsupervised neural network model, the UFN reasoning model, to implement the damage localization process.

The UFN reasoning model was proposed by Hung and Jan [26–28]. The UFN reasoning model consists of an unsupervised neural network with a fuzzy computing process. The UFN reasoning model is implemented in three steps which are briefly reviewed in the following subsections.

3.1. Measurement of similarities

The first step involves searching for instances that similar to the new instance ($\mathbf{Y}$) in the instance base ($\mathbf{U}_j$) according to their inputs (Y_i and $U_{j,i}$). The similarity measurement is implemented by calculating the degree of difference between two instances. The function of degree of difference is defined as

$$d_{Yj} = diff(Y_i, U_{j,i}) = \sum_{m=1}^{M} \alpha_m (x^m - u_j^m)^2 \tag{11}$$

where d_{Yj} denotes the discrepancy between the inputs of the new instance $\mathbf{Y}$ and the jth instance $\mathbf{U}_j$ in the instance base; α_m denotes predefined weight which represents the degree of importance for the mth decision variable in the input. After the values of d_{Yj} for all instances are calculated,

the degree of similarity of instances $\mathbf{Y}$ and $\mathbf{U}_j$ can be derived by the following fuzzy membership function.

$$\mu_{Yj} = f(d_{Yj}, R_{\max}, R_{\min}) = \begin{cases} 0 & \text{if } d_{Yj} \geqslant R_{\max} \\ \dfrac{R_{\max}R_{\min} - R_{\min}d_{Yj}}{(R_{\max} - R_{\min})d_{Yj}} & \text{if } R_{\min} < d_{Yj} < R_{\max} \\ 1 & \text{if } d_{Yj} \leqslant R_{\min} \end{cases} \tag{12}$$

The terms $R_{\max}$ and $R_{\min}$ define the upper and lower bounds of the relationship of similarity. In case the degree of difference is less than the upper bound $R_{\max}$, any two instances are treated as similar in some measure. Obviously, Equations (11) and (12) show that the smaller the discrepancy d_{Yj} is, the higher is the degree of similarity. Additionally, the upper bound $R_{\max}$ heavily influences the measurement of similarity. A large $R_{\max}$ implies a loose similar relationship between instances. On the other hand, a small $R_{\max}$ indicates that a strict similar relationship is adopted. In order to systematically determine the appropriate value of $R_{\max}$ a linear correlation analysis is employed. More details about the influence of $R_{\max}$ and the correlation analysis process can be seen in the references [26–28].

3.2. Generation of the fuzzy set of similar instances

The second step entails representing the fuzzy relationships among the new instance and its similar instances. The instances with the degree of difference smaller than $R_{\max}$ (i.e. $\mu > 0$) are extracted from the instance base as similar instances. Subsequently, the fuzzy set of 'similar to $\mathbf{Y}$' is then formed with the similar instances and their corresponding fuzzy membership values.

$$S_{\sup,Y} = \{S_1(\mu_1), S_2(\mu_2), \ldots, S_p(\mu_p), \ldots\} \tag{13}$$

where S_p is the pth similar instance to instance $\mathbf{Y}$; and μ_p is the corresponding fuzzy membership value.

3.3. Synthesis of the solution for new instance

Finally, the solution for instance $\mathbf{Y}$ is generated by synthesizing the outputs of similar instances according to their associated fuzzy membership value through the center of gravity (COG) method. The output Y_o of instance $\mathbf{Y}$ is defined as follows:

$$Y_o = \frac{\sum_{k=1}^{p} \mu_k S_{k,o}}{\sum_{k=1}^{p} \mu_k} \tag{14}$$

Figure 1 schematically portrays the three steps of the UFN reasoning.

Together with the theories of DLF and UFN reasoning model, this study makes use of the DLF as the input variables and the existence of the damaged site as the output vector to the UFN. Based on the analytic model, the ADLF for various possible damage cases can be calculated in advance. When the modal parameters of the structure are available, the damage location can then be assessed by matching the measured damage localization feature (MDLF) with the ADLF through the UFN reasoning.

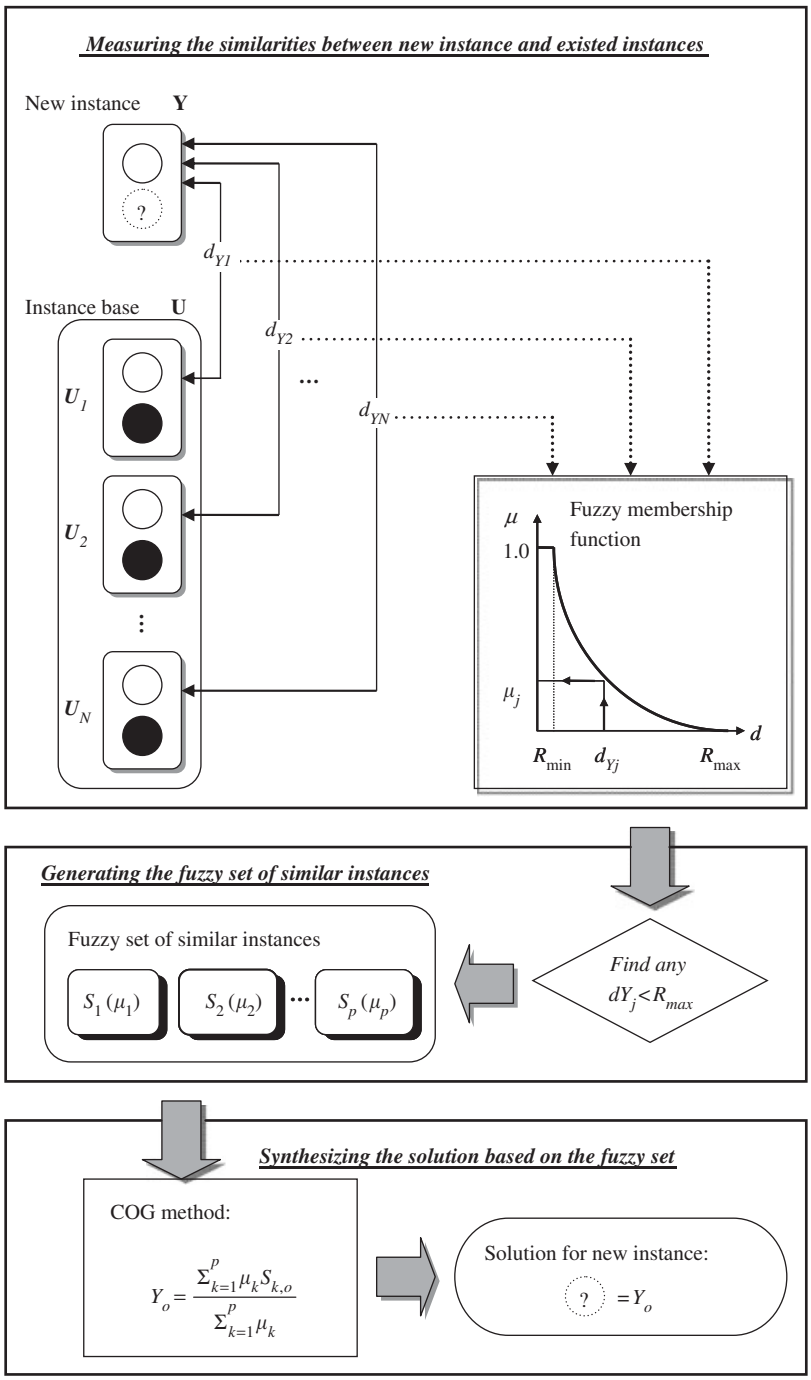

Figure 1. Process of the UFN reasoning (open and full circles represent the input and solution of the instance, respectively).

4. NUMERICAL STUDY

4.1. Introduction to the numerical example

A numerical example, a one-bay, five-storey shear plane frame structure, is presented herein to investigate the feasibility of the proposed damage detection procedures. The structural parameters for each floor are set to be the same, i.e. the mass $m_i = 2$ kg and the stiffness $k_i = 1500$ N/m ($i = 1$–5).

In this work, the damage cases are simulated by the reduction of storey stiffness of the first, second or third floor. Both single-site and multiple-site damage cases are discussed. Table I shows the characterizations of the simulated damage cases. Notably, the symbols Dam_k_i ($i = 1$–3) in Table I denote that the damage results in reduction of stiffness of k_i at single site (Cases 1–60). Similarly, the symbols $Dam\_k_i\&k_j$ ($i \neq j$) mean that the damages result in reduction of stiffness of k_i and k_j at multiple sites (Cases 61–132). The modal parameters of the undamaged and damaged cases are obtained through the analytic model.

4.2. Arrangement of the inputs and outputs for the UFN

The modal data for each damage case listed in Table I is yielding based on the analytic model and is then compared with the modal data for undamaged model to obtain the changes in modal eigenvalues and mode shapes. For each damage case, the ADLF can be derived using the left-hand-side of Equation (10). For the UFN, the ADLF is treated as input variable of the neural network. Moreover, the output vector for the UFN represents the condition of the structural elements. If the element is damaged, the value in the output vector is set to 1 to the associate element; otherwise, the value is set to be 0 to indicate an undamaged element. For example, the output vector for damage class $Dam\_k_1\&k_3$ is set to be [1, 0, 1].

4.3. DLF of the numerical model

Figures 2–7, respectively, show the contour maps of the DLF, which are obtained via the left-hand-side of Equation (10), for each simulated damage class in this paper. The horizontal and vertical axes represent the number of the measured degrees-of-freedom (dofs) and of the obtained modes, respectively. For example, the contour maps (a) of Figures 2–7 are based on the values of $\Delta\phi/\Delta\lambda_1$; and the contour maps (b) of Figures 2–7 are based on the values of $\Delta\phi/\Delta\lambda_2$. Additionally, the darker the shades in the figures are, the larger are the values of DLF.

Table I. Characterizations of simulated damage cases.

Damage class	Damage level	Number of damage cases
Dam_k_1	2–40% (every 2%)	Cases 1–20
Dam_k_2	2–40% (every 2%)	Cases 21–40
Dam_k_3	2–40% (every 2%)	Cases 41–60
$Dam\_k_1\&k_2$	5–30% for k_1 (every 5%) 5–30% for k_2 (every 5%)	Cases 61–96
$Dam\_k_1\&k_3$	5–30% for k_1 (every 5%) 5–30% for k_3 (every 5%)	Cases 97–132

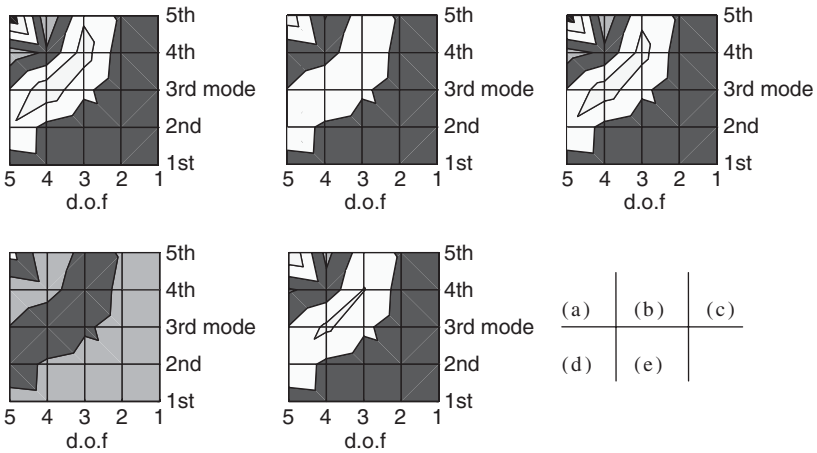

Figure 2. Contour maps of the DLF for the damage class Dam_k_1 with 20% damage extent.

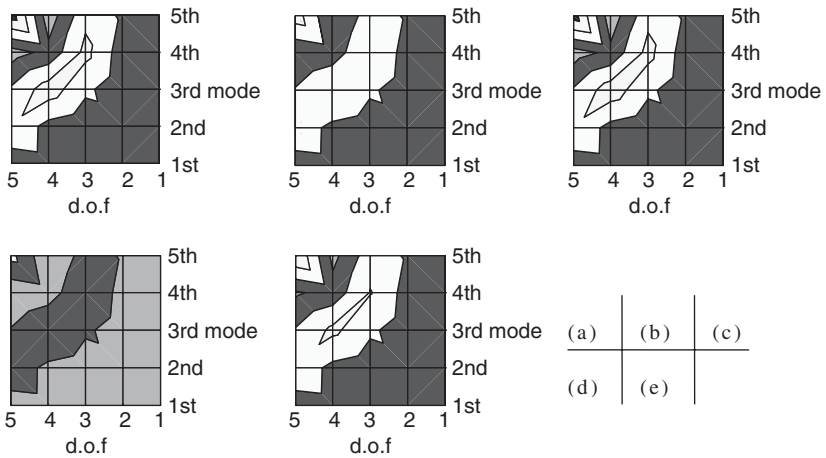

Figure 3. Contour maps of the DLF for the damage class Dam_k_1 with 26% damage extent.

As mentioned previously, Equation (10) depends on damage location only. Consequently, the DLFs, shown in Figures 2 and 3 for the same damage class, but with different damage levels, are almost the same. Moreover, Figures 3–7 show that the DLF for different damage classes are distinguishable. It is interested to mention that, although the DLFs for Dam_k_3 and $Dam\_k_1\&k_3$ class (Figures 5 and 7) are distinguishable, there exists certain degree of similarity between each other. This outcome is rational because these two damage classes are both damaged for stiffness k_3.

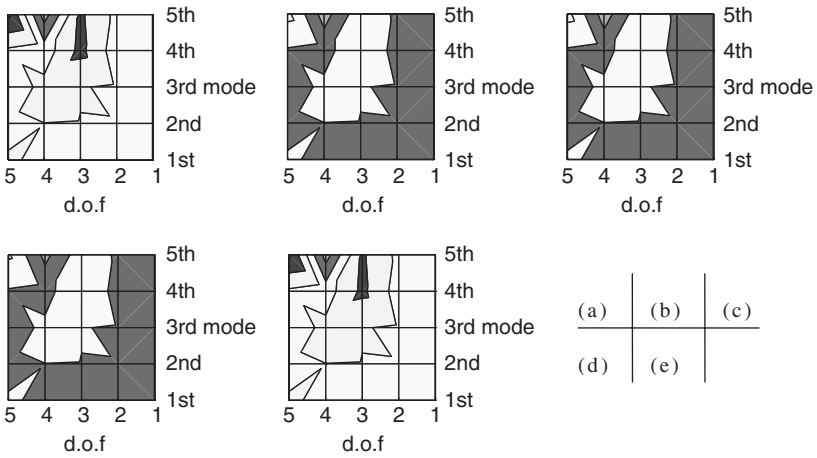

Figure 4. Contour maps of the DLF for the damage class Dam_k_2 with 20% damage extent.

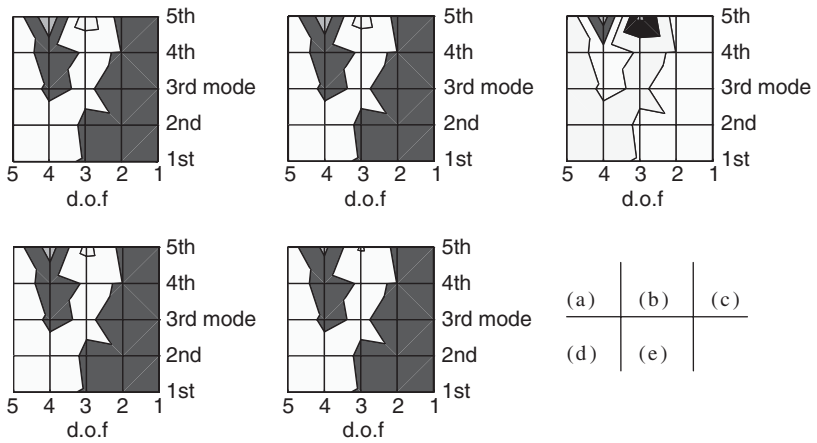

Figure 5. Contour maps of the DLF for the damage class Dam_k_3 with 20% damage extent.

4.4. *Training of the UFN*

The ADLF, together with the related structural element condition for each damage case, is treated as an instance. Hence, 132 instances are obtained. Note that, Cases 1–10 are instances of damage class Dam_k_1; Cases 21–40 are instances of damage class Dam_k_2; Cases 41–60 are instances of damage class Dam_k_3; Cases 61–96 are instances of damage class $Dam\_k_1\&k_2$; Cases 97–132 are instances of damage class $Dam\_k_1\&k_3$. These 132 instances are separated into two sets: the training set and the testing set. For UFN, the training set is also named as an

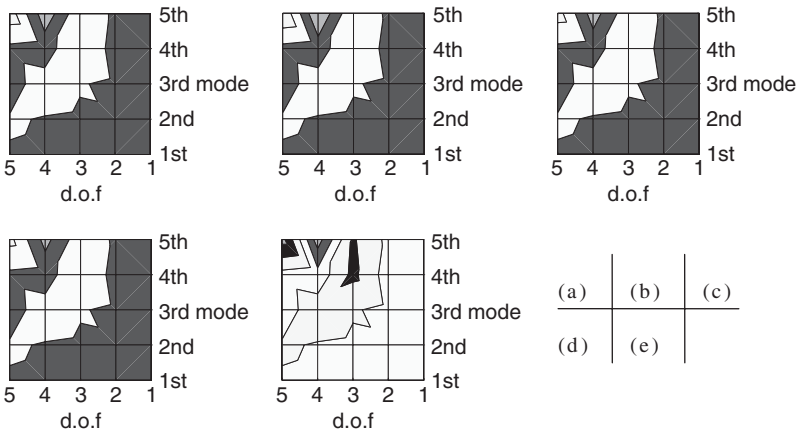

Figure 6. Contour maps of the DLF for the damage class $Dam\_k_1\&k_2$ with 20% damage extent.

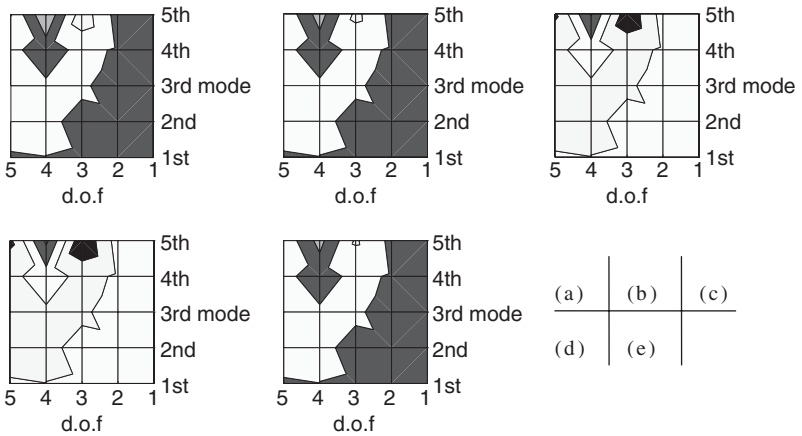

Figure 7. Contour maps of the DLF for the damage class $Dam\_k_1\&k_3$ with 20% damage extent.

instance base. A total of 18 instances that randomly selected from the 132 instances are collected as testing set to verify the performance of the UFN reasoning model. Table II lists some characterizations about the testing instances. Furthermore, the input values of the testing instances are treated as MDLF. Hence, the output of the testing instances will be generated through the UFN reasoning by matching the MDLF and ADLF.

Before verification of the testing instances, the UFN is trained first. The training of the UFN is to determine the upper bound $R_{\max}$ for the membership function and the weights α_m for the similarity measurement. According to Hung and Jan [28], an appropriate value of $R_{\max}$ is selected when the accumulative correlation coefficient (ACC) exceeds 0.8. Herein, the corresponding $R_{\max}$ that makes the accumulative correlation coefficient exceeds 0.85 is adopted

Table II. Characterizations of the verified instances.

Instance	Output vector	Damage class	Damage severity (%)
1	[1, 0, 0]	Dam_k_1	8
2	[1, 0, 0]	Dam_k_1	26
3	[0, 1, 0]	Dam_k_2	6
4	[0, 1, 0]	Dam_k_2	22
5	[0, 0, 1]	Dam_k_3	12
6	[0, 0, 1]	Dam_k_3	24
7	[1, 1, 0]	$Dam\_k_1\&k_2$	5 and 10
8	[1, 1, 0]	$Dam\_k_1\&k_2$	10 and 10
9	[1, 1, 0]	$Dam\_k_1\&k_2$	15 and 10
10	[1, 1, 0]	$Dam\_k_1\&k_2$	20 and 20
11	[1, 1, 0]	$Dam\_k_1\&k_2$	25 and 15
12	[1, 1, 0]	$Dam\_k_1\&k_2$	30 and 20
13	[1, 0, 1]	$Dam\_k_1\&k_3$	5 and 15
14	[1, 0, 1]	$Dam\_k_1\&k_3$	10 and 15
15	[1, 0, 1]	$Dam\_k_1\&k_3$	15 and 20
16	[1, 0, 1]	$Dam\_k_1\&k_3$	20 and 10
17	[1, 0, 1]	$Dam\_k_1\&k_3$	25 and 25
18	[1, 0, 1]	$Dam\_k_1\&k_3$	30 and 15

for more strict. The value of $R_{\max}$ is determined to be 0.01 and the values of α_m are all set to be constant one.

4.5. Evaluation of the diagnostic accuracy

An index, SDD (degree of successful diagnosis), is used to evaluate the accuracy of the predicted outputs of the networks. Herein, the values 0.2 and 0.8 are selected to be the threshold of the confirmed undamaged and damaged site, respectively. Restated, the generated output value of the network that less than 0.2 or larger than 0.8 is assumed to be a successful diagnosis for undamaged or damaged case. The SDD is calculated by the following equation.

$$\mathrm{SDD} = \frac{N_{\mathrm{SD}}}{N_{\mathrm{ED}}} \times 100\% \tag{15}$$

where N_{SD} is the total number of the successful diagnosis; N_{ED} is the total number of the expected diagnosis. The value SDD equals to 100% if the identifications of damage location(s) for all testing cases are correct; otherwise, a value 0% represents that wrong damage localization happens for every testing case.

5. RESULTS AND DISCUSSIONS

5.1. Identification results without noise polluted in DLF

Based on the working parameters generated from the training process, the verified results of the 18 testing instances are obtained and listed in Table III. According to the verified results, the UFN reasoning model shows excellent agreement in localization of the damage (SDD = 100%).

Table III. Diagnostic results via UFN (without noise).

Instance	True vector	UFN outputs	Similar instances
1	[1, 0, 0]	[1.00, 0.01, 0.02]	1,2,3,5,6,7,8,9,10,11,12,14,15,16,17,18,19,20, 73,79,80,85,86,91,92,93,95,115,121,127,128
2	[1, 0, 0]	[1.00, 0.00, 0.00]	1,2,3,5,6,7,8,9,10,11,12,14,15,16,17,18,19,20, 79,85,86,91,92,93,115,121,127,128
3	[0, 1, 0]	[0.00, 1.00, 0.00]	21,22,24,25
4	[0, 1, 0]	[0.00, 1.00, 0.00]	28,29,30,32,33,34,35
5	[0, 0, 1]	[0.00, 0.00, 1.00]	41,42,43,44,45,47,48,49,50,51,52
6	[0, 0, 1]	[0.00, 0.00, 1.00]	47,48,49,50,51,52,53,54,56,57,58
7	[1, 1, 0]	[1.00, 1.00, 0.00]	61,63,64,65,69,70,71,72
8	[1, 1, 0]	[1.00, 1.00, 0.00]	61,67,69,70,71,72,75,76,77,78,80,81,83,84,88, 89,90,95,96
9	[1, 1, 0]	[1.00, 0.99, 0.00]	61,67,69,70,71,72,73,75,76,77,78,79,80,81,83, 84,85,86,88,89,90,92,93,95,96,103,109,116,122
10	[1, 1, 0]	[1.00, 1.00, 0.00]	61,67,69,70,71,72,73,75,76,77,78,79,80,81,83, 84,85,86,88,89,90,92,93,95,96,109
11	[1, 1, 0]	[1.00, 0.99, 0.01]	1,2,3,5,6,67,73,75,76,77,79,80,81,83,84,85,88, 89,92,93,95,96,103,109,115,121,122,127,128
12	[1, 1, 0]	[1.00, 0.98, 0.02]	1,2,3,6,7,9,10,67,73,75,76,77,79,80,81,83,84,85, 86,89,90,91,92,95,96,109,115,121,122,127,128
13	[1, 0, 1]	[0.99, 0.00, 1.00]	56,57,58,59,98,100,101,102,106,107,108
14	[1, 0, 1]	[1.00, 0.00, 1.00]	97,98,104,106,107,108,111,113,114,118,119, 120,126
15	[1, 0, 1]	[1.00, 0.00, 1.00]	97,98,104,106,107,108,110,111,113,114,117, 118,119,120,124,126,131,132
16	[1, 0, 1]	[1.00, 0.01, 0.99]	67,73,79,80,81,86,92,93,103,104,109,110,115, 117,118,121,122,123,126,127,128,130,131,132
17	[1, 0, 1]	[1.00, 0.00, 1.00]	97,103,104,110,111,113,114,117,118,119,120, 122,123,124,126,130,131,132
18	[1, 0, 1]	[1.00, 0.02, 0.98]	67,73,79,80,85,86,91,92,93,103,109,110,115, 117,118,121,122,123,124,127,128,130,131,132

It is interested to mention that, for testing instance 2, Cases 79 and 115 in the instance base are found to be 'similar' to this testing instance, even the damage class of the testing instance 2 (i.e. Dam_k_1) and those of Cases 79 and 115 (i.e. $Dam\_k_1\&k_2$ and $Dam\_k_1\&k_3$, respectively) are different. However, the UFN reasoning model can still generate the correct result. The same situation also occurs for the other testing instances such as testing instances 1, 9, 10, 11, 12, 13, 16, and 18.

Because the upper bound $R_{\max}$ is selected when the accumulative correlation coefficient exceeds 0.85, an explanation is made that the found similar instances have more than 85% correlation with the testing instance. Restated, when the solution for a testing instance is obtained through the UFN, the degree of reliability of the solved solution is more than 85%. Consequently, the output values of the UFN have a further meaning. For example, the output vector for the testing instance 18 is [1.00, 0.02, 0.98] which means that the possibilities of the elemental damage are 100, 2, and 98, respectively, based on the reliability of 85%.

Table IV. Diagnostic results via UFN (with various noise levels).

Instance	UFN output vector		
	1% noise	3% noise	4% noise
1	[1.00, 0.08, 0.04]	[1.00, 0.11, 0.01]	[1.00, 0.19, 0.04]
2	[1.00, 0.01, 0.00]	[1.00, 0.01, 0.01]	[1.00, 0.04, 0.02]
3	[0.00, 1.00, 0.00]	[0.00, 1.00, 0.00]	[NA, NA, NA] ([0.00, 1.00, 0.00])*
4	[0.00, 1.00, 0.00]	[0.00, 1.00, 0.00]	[0.00, 1.00, 0.00]
5	[0.00, 0.00, 1.00]	[0.00, 0.00, 1.00]	[0.00, 0.00, 1.00]
6	[0.00, 0.00, 1.00]	[0.00, 0.00, 1.00]	[0.04, 0.00, 1.00]
7	[1.00, 1.00, 0.00]	[1.00, 1.00, 0.00]	[1.00, 1.00, 0.00]
8	[1.00, 1.00, 0.00]	[1.00, 1.00, 0.00]	[1.00, 1.00, 0.00]
9	[1.00, 1.00, 0.00]	[1.00, 0.99, 0.00]	[1.00, 1.00, 0.00]
10	[1.00, 1.00, 0.00]	[1.00, 1.00, 0.00]	[1.00, 1.00, 0.00]
11	[1.00, 0.99, 0.01]	[1.00, 0.98, 0.02]	[1.00, 0.98, 0.02]
12	[1.00, 0.98, 0.02]	[1.00, 0.97, 0.02]	[1.00, 0.98, 0.01]
13	[0.99, 0.00, 1.00]	[0.99, 0.00, 1.00]	[0.87, 0.00, 1.00]
14	[1.00, 0.00, 1.00]	[1.00, 0.00, 1.00]	[1.00, 0.00, 1.00]
15	[1.00, 0.00, 1.00]	[1.00, 0.00, 1.00]	[1.00, 0.00, 1.00]
16	[1.00, 0.01, 0.99]	[1.00, 0.01, 0.99]	[1.00, 0.03, 0.97]
17	[1.00, 0.00, 1.00]	[1.00, 0.00, 1.00]	[1.00, 0.00, 1.00]
18	[1.00, 0.02, 0.98]	[1.00, 0.02, 0.98]	[1.00, 0.03, 0.97]
SDD	100%	100%	94.4%

NA: data not available (no similar instance found).
*When the most similar instance is chosen.

5.2. *Verified results with noise polluted in DLF*

In order to make the proposed damage detection method more practical, the noise effect is considered in the verification. In this study, the mode shapes are noise polluted with various levels of random signals. The contaminated signal is represented as [29]

$$\bar{\phi}_{ij} = \phi_{ij}(1 + r_i^{\phi} l^{\phi} |\phi_{\max,j}|) \tag{16}$$

where $\bar{\phi}_{ij}$ and ϕ_{ij} are the mode shape components of the jth mode at the ith dof with and without noise, respectively; r_i^{ϕ} is the random number with zero mean and unit variance; l^{ϕ} is the noise level; and $\phi_{\max,j}$ is the largest component in the jth mode shape.

Table IV shows the diagnostic results of the testing instances of which the mode shapes are contaminated with 1, 3, and 4 random noise, respectively. As mentioned previously, the values 0.2 and 0.8 are used to be the threshold of the confirmed undamaged and damaged site. The UFN outputs, listed in Table IV, also show the correct diagnosis about the damage location except for the testing instance 3 with 4% contaminated noise. The SDD for the 1 and 3% measured noise conditions are both 100%, and the SDD for the 4% measured noise condition can still reach 94.4%. The reason why the UFN cannot generate an output vector in the condition of 4% measured noise is that the matching process finds no similar instances in the instance base within 85% degree of correlation. To overcome this problem, two strategies are

Table V. Diagnostic results via BPN.

Instance	BPN output vector	
	Without noise	1% noise
1	[1.00, 0.00, 0.00]	[1.00, 0.00, 0.44*]
2	[1.00, 0.00, 0.00]	[1.00, 0.00, 0.00]
3	[0.00, 1.00, 0.00]	[0.00, 1.00, 0.00]
4	[0.00, 1.00, 0.00]	[0.00, 1.00, 0.00]
5	[0.00, 0.00, 1.00]	[0.00, 0.00, 1.00]
6	[0.00, 0.00, 1.00]	[0.00, 0.00, 1.00]
7	[1.00, 1.00, 0.01]	[1.00, 1.00, 0.00]
8	[1.00, 1.00, 0.00]	[1.00, 1.00, 0.00]
9	[1.00, 1.00, 0.00]	[1.00, 1.00, 0.00]
10	[1.00, 1.00, 0.00]	[1.00, 1.00, 0.00]
11	[1.00, 1.00, 0.00]	[1.00, 1.00, 0.00]
12	[1.00, 1.00, 0.00]	[1.00, 1.00, 0.00]
13	[1.00, 0.00, 1.00]	[1.00, 0.00, 1.00]
14	[1.00, 0.01, 1.00]	[1.00, 0.00, 1.00]
15	[1.00, 0.00, 1.00]	[1.00, 0.00, 1.00]
16	[1.00, 0.00, 1.00]	[1.00, 0.00, 1.00]
17	[1.00, 0.00, 1.00]	[1.00, 0.00, 1.00]
18	[1.00, 0.00, 1.00]	[1.00, 0.00, 1.00]
SDD	100%	98.1%

*Wrong diagnosis.

employed in this work. One is to loose the degree of correlation (i.e. to select a larger value of $R_{\max}$). The other is to select the instance with the smallest degree of difference as the similar instance to generate the output vector. For example, if the second strategy is adopted, the output vector of the unsolved testing instance 3 will be [0.00, 1.00, 0.00], and the SDD would be 100% which means the identifications of the damage locations are undoubtedly successful.

5.3. Comparison with the BPN

In this study, the same data set is also processed through a supervised neural network for the sake of comparison. A BPN with the topology of 100-53-3 (i.e. 100 inputs, one hidden layer with 53 hidden nodes, and 3 outputs) is adopted. The training is terminated when the system error of the BPN is smaller than that of the UFN. The diagnostic results of the instances without and with noise are listed in Table V. It is evident that the BPN can precisely detect the location of the damaged element when the data set is not polluted. However, even with small intensity of noise (with 1% noise), the BPN could possibly generate the incorrect damage localization. For example, the BPN outputs for the testing instance 1 indicate that the damage occurred at the first and third storey columns, while the actual damage occurred at the first storey columns only. According to the numerical example, although the system error of the network output for BPN is slightly smaller than that for UFN, it is important to mention that BPN is more inflexible due to the possibility of incorrect diagnosis when dealing with measured noise. Nevertheless, it is

Table VI. Diagnostic results of using incomplete modal data via UFN.

Instance	UFN output vector		
	Without noise	1% noise	3% noise
1	[1.00, 0.01, 0.04]	[1.00, 0.13, 0.07]	[1.00, 0.16, 0.12]
2	[1.00, 0.00, 0.00]	[1.00, 0.02, 0.02]	[1.00, 0.08, 0.03]
3	[0.00, 1.00, 0.00]	[0.00, 1.00, 0.00]	[NA, NA, NA] ([0.00, 1.00, 0.00])*
4	[0.00, 1.00, 0.00]	[0.00, 1.00, 0.00]	[0.00, 1.00, 0.00]
5	[0.00, 0.00, 1.00]	[0.00, 0.00, 1.00]	[0.03, 0.00, 1.00]
6	[0.00, 0.00, 1.00]	[0.01, 0.00, 1.00]	[0.01, 0.00, 1.00]
7	[1.00, 1.00, 0.00]	[1.00, 1.00, 0.00]	[1.00, 1.00, 0.00]
8	[1.00, 1.00, 0.00]	[1.00, 1.00, 0.00]	[1.00, 1.00, 0.00]
9	[1.00, 0.99, 0.00]	[1.00, 0.99, 0.00]	[0.98, 1.00, 0.00]
10	[1.00, 1.00, 0.00]	[1.00, 1.00, 0.00]	[1.00, 1.00, 0.00]
11	[1.00, 0.98, 0.00]	[1.00, 0.97, 0.00]	[1.00, 0.99, 0.00]
12	[1.00, 0.98, 0.00]	[1.00, 0.97, 0.00]	[1.00, 1.00, 0.00]
13	[0.94, 0.00, 1.00]	[0.94, 0.00, 1.00]	[0.92, 0.00, 1.00]
14	[1.00, 0.00, 1.00]	[1.00, 0.00, 1.00]	[1.00, 0.00, 1.00]
15	[1.00, 0.00, 1.00]	[1.00, 0.00, 1.00]	[1.00, 0.00, 1.00]
16	[1.00, 0.00, 0.96]	[1.00, 0.00, 0.94]	[1.00, 0.00, 0.96]
17	[1.00, 0.00, 1.00]	[1.00, 0.00, 1.00]	[1.00, 0.00, 1.00]
18	[1.00, 0.00, 0.94]	[1.00, 0.00, 0.94]	[1.00, 0.00, 0.90]
SDD	100%	100%	94.4% (100%)*

NA: data not available (no similar instance found).*When the most similar instance is chosen for NA situation.

clear from this study and other researches that neural network is a promising technique in the damage detection of structures.

5.4. Verified results when using the incomplete modal data

In practical situation, only a truncated set of modal frequencies can be obtained experimentally. Besides, only partial dof with respect to the total dof of a real structural would be monitored, which results in incomplete measured mode shapes. In this section, the effect of using incomplete modal data (truncated set of modal frequencies and incomplete mode shapes) is investigated to verify the robustness of the UFN in damage detection. Assumed that only the first, second, and third modes can be obtained and only the first, third, and fifth dofs of the structure are monitored. Hence, the number of the input variables is substantially reduced from 100 to 18.

Table VI shows the verified results of the UFN in damage detection while using the incomplete modal data with/without noise. It is clear from the table that, even with the measured noise and partial modal data, the UFN still can locate the damaged sites satisfactorily. The SDD for the conditions of 0, 1, and 3% measured noise are 100, 100, and 94.4%, respectively. The results shown in Sections 5.2 and 5.4 validate that the proposed damage detection approach is robust and flexible when dealing with the measured noise and (or) incomplete modal data situations.

6. CONCLUSIONS

This investigation proposes a novel method of damage detection, based on structural modal data and an unsupervised fuzzy neural network. After obtaining the damage feature based on structure modal data, the damage site is located by matching two sets of damage features, analytic damage localization feature (ADLF) and measured damage localization feature (MDLF). The matching process is implemented using the UFN reasoning model. From the analytic model, the ADLF must be calculated in advance. By deploying sensors on the structure, the MDLF can be obtained and inputted to the UFN reasoning model to locate the damage.

A numerical example involving a five-storey shear-building structure was presented to demonstrate the feasibility of the proposed approach. To improve the practicality of the proposed damage detection method, the effects of measured noise and incomplete modal data are introduced to examine the feasibility of the proposed detection approach. Additionally, a commonly used supervised neural network, BPN, in the network-based damage detection method is also introduced, and its performance is compared with that of the UFN. Some conclusions are made based on the simulation results demonstrated in this work.

1. The matching process based on the damage localization feature is a form of pattern recognition. From the verification results, the unsupervised neural network (UFN in this study for example) appears superior to the BPN in dealing with the damage localization. However, more investigations (such as training algorithm, network topology, etc.) need to be available concerning the BPN.
2. Even with noise contamination in the modal parameters, the UFN still locate the damage sufficiently accurately, although the BPN would likely make an incorrect diagnosis in such circumstances.
3. The UFN achieves effective damage localization when using a truncated set of modal frequencies and incomplete mode shapes.
4. The use of the fuzzy set in UFN increased the robustness and flexibility of the detection. The proposed approaches display excellent promise for damage localization.

ACKNOWLEDGEMENT

The work reported herein was partially supported by the National Science Council, R.O.C. through research grant NSC90-2211-E-009-031. This support is gratefully acknowledged.

REFERENCES

1. Kim JT, Stubbs N. Damage detection in offshore jacket structures from limited modal information. *International Journal of Offshore and Polar Engineering* 1995; **5**(1):58–66.
2. Topole KG, Stubbs N. Nondestructive damage evaluation in complex structures from a minimum of modal parameters. *The International Journal of Analytical and Experimental Modal Analysis* 1995; **10**(2):95–104.
3. Stubbs N, Topole KG. A damage localization algorithm for nonlinear structures. In: Natke GR, Yao JTP (eds) *Safety Evaluation Based on Identification Approach Related to Time-variant and Nonlinear Structures*. Vieweg 1993; 93–106.
4. Wen YK. Intelligent structures 2: monitoring and control. *Proceedings of the International Workshop on Intelligent Systems*, New York, 1992;1–10.

5. Cawley P, Adams RD. The location of defects in structures from measurements of natural frequencies. *Journal of Strain Analysis* 1979; **14**(2):49–57.
6. Penny JET, Wilson D, Friswell MI. Damage location in structures using vibration data. *Proceedings of the 11th International Modal Analysis Conference*, Kissimee, 1993; 861–867.
7. Contursi T, Messina A, Williams EJ. A multiple-damage location assurance criterion based on natural frequency changes. *Journal of Vibration and Control* 1998; **4**(5):619–663.
8. Messina A, Jones IA, Williams EJ. Damage detection and localisation using natural frequency changes. *Proceedings of the Conference on Identification in Engineering Systems*, Swansea, 1996; 67–76.
9. Messina A, Williams EJ, Contursi T. Structural damage detection by a sensitivity and statistical-based method. *Journal of Sound and Vibration* 1998; **216**(5):791–808.
10. West WM. Illustration of the use of modal assurance criterion to detect structural changes in an orbiter test specimen. *Proceedings of the 4th International Modal Analysis Conference*, 1986; 1–5.
11. Lieven NAJ, Ewins DJ. Spatial correlation of mode shapes, the coordinate modal assurance criterion (COMAC). *Proceedings of the 5th International Modal Analysis Conference*, 1988; 690–695.
12. Biswas M, Pandey AK, Samman MM. Diagnosis experiment spectral/modal analysis of highway bridges. *The International Journal of Analytical and Experimental Modal Analysis* 1990; **5**(1):33–42.
13. Topole KG, Stubbs N. Non-destructive damage evaluation of a structure from limited modal parameters. *Earthquake Engineering and Structural Dynamics* 1995; **24**(12):1427–1436.
14. Shi ZY, Law SS, Zhang LM. Damage localization by directly using incomplete mode shapes. *Journal of Engineering Mechanics* (ASCE) 2000; **126**(6):656–660.
15. Hearn G, Testa RB. Modal analysis for damage detection in structures. *Journal of Structural Engineering* (ASCE) 1991; **117**(10):3042–3063.
16. Shi ZY, Law SS, Zhang LM. Structural damage localization from modal strain energy change. *Journal of Sound and Vibration* 1998; **218**(5):825–844.
17. Masri SF, Chassiakos AG, Caughey TK. Identification of nonlinear dynamic systems using neural networks. *Journal of Applied Mechanics* 1993; **60**:123–133.
18. Ghaboussi J, Garrett JH, Wu X. Knowledge-based modeling of material behavior with neural networks. *Journal of Engineering Mechanics* (ASCE) 1991; **117**(1):132–153.
19. Wu X, Ghaboussi J, Garrett Jr JH. Use of neural networks in detection of structural damage. *Computers and Structures* 1992; **42**(4):649–659.
20. Elkordy MF. *Application of Neural Networks in Structural Damage Diagnosis and Condition Monitoring*. UMI Dissertation Services, A Bell & Howell Company, 1992.
21. Zhao J, Ivan JN, DeWolf JT. Structural damage detection using artificial neural networks. *Journal of Infrastructure Systems* (ASCE) 1998; **4**(2):93–101.
22. Masri SF, Nakamura M, Chassiakos AG, Caughey TK. Neural network approach to the detection of changes in structural parameters. *Journal of Engineering Mechanics* (ASCE) 1996; **122**(4):350–360.
23. Masri SF, Smyth AW, Chassiakos AG, Caughey TK, Hunter NF. Application of neural networks for detection of changes in nonlinear systems. *Journal of Engineering Mechanics* (ASCE) 2000; **126**(7):666–676.
24. Huang CS, Hung SL, Wen CM, Tu TT. A neural network approach for structural identification and diagnosis of a building from seismic response data. *Earthquake Engineering and Structural Dynamics* 2003; **32**(2):187–206.
25. Lam HF, Ko JM, Wong CW. Localization of damaged structural connections based on experimental modal and sensitivity analysis. *Journal of Sound and Vibration* 1998; **210**(1):91–115.
26. Hung SL, Jan JC. Machine learning in engineering design: an unsupervised fuzzy neural network learning model. *Proceedings of the Conference on Intelligent Information Systems, IEEE Computer Society*, California, 1997; 156–160.
27. Hung SL, Jan JC. Machine learning in engineering analysis and design: an integrated fuzzy neural network learning model. *Computer-Aided Civil and Infrastructure Engineering* 1999; **14**:207–219.
28. Hung SL, Jan JC. Augmented IFN Learning Model. *Journal of Computing in Civil Engineering* (ASCE) 2000; **14**(1):15–22.
29. Shi ZY, Law SS, Zhang LM. Structural damage detection from modal strain energy change. *Journal of Engineering Mechanics* (ASCE) 2000; **126**(12):1216–1223.

